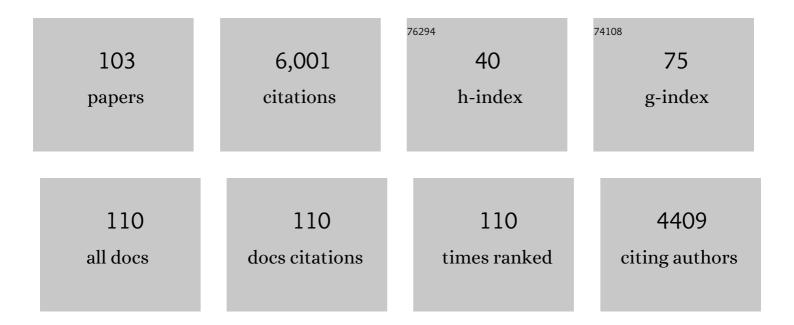
## William D A Rickard

List of Publications by Year in descending order

Source: https://exaly.com/author-pdf/6280547/publications.pdf Version: 2024-02-01



#	Article	IF	CITATIONS
1	Costs and carbon emissions for geopolymer pastes in comparison to ordinary portland cement. Journal of Cleaner Production, 2011, 19, 1080-1090.	4.6	1,221
2	A comparison between different foaming methods for the synthesis of light weight geopolymers. Ceramics International, 2014, 40, 13891-13902.	2.3	228
3	Thermal analysis of geopolymer pastes synthesised from five fly ashes of variable composition. Journal of Non-Crystalline Solids, 2012, 358, 1830-1839.	1.5	200
4	Assessing the suitability of three Australian fly ashes as an aluminosilicate source for geopolymers in high temperature applications. Materials Science & Engineering A: Structural Materials: Properties, Microstructure and Processing, 2011, 528, 3390-3397.	2.6	193
5	Preparation and thermal properties of fire resistant metakaolin-based geopolymer-type coatings. Journal of Non-Crystalline Solids, 2011, 357, 1399-1404.	1.5	185
6	Preparation of metakaolin based geopolymer coatings on metal substrates as thermal barriers. Applied Clay Science, 2009, 46, 265-270.	2.6	164
7	Performance of fibre reinforced, low density metakaolin geopolymers under simulated fire conditions. Applied Clay Science, 2013, 73, 71-77.	2.6	156
8	Determination of the reactive component of fly ashes for geopolymer production using XRF and XRD. Fuel, 2010, 89, 3683-3692.	3.4	155
9	Determining the Reactivity of a Fly Ash for Production of Geopolymer. Journal of the American Ceramic Society, 2009, 92, 881-887.	1.9	138
10	Thermal Character of Geopolymers Synthesized from Class F Fly Ash Containing High Concentrations of Iron and αâ€Quartz. International Journal of Applied Ceramic Technology, 2010, 7, 81-88.	1.1	126
11	The effect of organic and inorganic fibres on the mechanical and thermal properties of aluminate activated geopolymers. Composites Part B: Engineering, 2015, 76, 218-228.	5.9	122
12	Fly ash based geopolymer thin coatings on metal substrates and its thermal evaluation. Journal of Hazardous Materials, 2010, 180, 748-752.	6.5	120
13	Thermo-mechanical and microstructural characterisation of sodium-poly(sialate-siloxo) (Na-PSS) geopolymers. Journal of Materials Science, 2007, 42, 3117-3123.	1.7	101
14	Quantification of the Extent of Reaction of Metakaolin-Based Geopolymers Using X-Ray Diffraction, Scanning Electron Microscopy, and Energy-Dispersive Spectroscopy. Journal of the American Ceramic Society, 2011, 94, 2663-2670.	1.9	101
15	High temperature behaviour of ambient cured alkali-activated materials based on ladle slag. Cement and Concrete Research, 2013, 43, 51-61.	4.6	101
16	Room temperature alkali activation of fly ash: The effect of Na 2 O/SiO 2 ratio. Construction and Building Materials, 2014, 69, 262-270.	3.2	98
17	Performance of solid and cellular structured fly ash geopolymers exposed to a simulated fire. Cement and Concrete Composites, 2014, 48, 75-82.	4.6	97
18	Nanoscale gold clusters in arsenopyrite controlled by growth rate not concentration: Evidence from atom probe microscopy. American Mineralogist, 2016, 101, 1916-1919.	0.9	94

#	Article	IF	CITATIONS
19	Nanogeochronology of discordant zircon measured by atom probe microscopy of Pb-enriched dislocation loops. Science Advances, 2016, 2, e1601318.	4.7	86
20	Atom Probe Tomography: Development and Application to the Geosciences. Geostandards and Geoanalytical Research, 2020, 44, 5-50.	1.7	84
21	Polarization-Induced Interface and Sr Segregation of <i>in Situ</i> Assembled La <sub>0.6</sub> Sr <sub>0.4</sub> Co <sub>0.2</sub> Fe <sub>0.8</sub> O <sub>3â~îî</sub> Electrodes on Y <sub>2</sub> O <sub>3</sub> –ZrO <sub>2</sub> Electrolyte of Solid Oxide Fuel Cells. ACS Applied Materials &: Interfaces. 2016. 8. 31729-31737.	4.0	82
22	In-situ thermo-mechanical testing of fly ash geopolymer concretes made with quartz and expanded clay aggregates. Cement and Concrete Research, 2016, 80, 33-43.	4.6	81
23	Impact of activator type on the immobilisation of lead in fly ash-based geopolymer. Journal of Hazardous Materials, 2016, 305, 59-66.	6.5	76
24	Thermally Induced Microstructural Changes in Fly Ash Geopolymers: Experimental Results and Proposed Model. Journal of the American Ceramic Society, 2015, 98, 929-939.	1.9	74
25	Direct application of cobaltite-based perovskite cathodes on the yttria-stabilized zirconia electrolyte for intermediate temperature solid oxide fuel cells. Journal of Materials Chemistry A, 2016, 4, 17678-17685.	5.2	70
26	Suppressed Sr segregation and performance of directly assembled La0.6Sr0.4Co0.2Fe0.8O3-δoxygen electrode on Y2O3-ZrO2 electrolyte of solid oxide electrolysis cells. Journal of Power Sources, 2018, 384, 125-135.	4.0	69
27	Bayer-geopolymers: An exploration of synergy between the alumina and geopolymer industries. Cement and Concrete Composites, 2013, 41, 29-33.	4.6	67
28	Mechanisms of deformation-induced trace element migration in zircon resolved by atom probe and correlative microscopy. Geochimica Et Cosmochimica Acta, 2016, 195, 158-170.	1.6	64
29	Microstructural constraints on the mechanisms of the transformation to reidite in naturally shocked zircon. Contributions To Mineralogy and Petrology, 2017, 172, 1.	1.2	64
30	Determination of amorphous phase levels in Portland cement clinker. Powder Diffraction, 2002, 17, 178-185.	0.4	59
31	Strategies to control the high temperature shrinkage of fly ash based geopolymers. Thermochimica Acta, 2014, 580, 20-27.	1.2	59
32	Thermal properties of spray-coated geopolymer-type compositions. Journal of Thermal Analysis and Calorimetry, 2012, 107, 287-292.	2.0	51
33	Smart utilization of cobaltite-based double perovskite cathodes on barrier-layer-free zirconia electrolyte of solid oxide fuel cells. Journal of Materials Chemistry A, 2016, 4, 19019-19025.	5.2	51
34	Dolomite: a low cost thermochemical energy storage material. Journal of Materials Chemistry A, 2019, 7, 1206-1215.	5.2	50
35	Nb and Pd co-doped La0.57Sr0.38Co0.19Fe0.665Nb0.095Pd0.05O3-Î <sup>^</sup> as a stable, high performance electrode for barrier-layer-free Y2O3-ZrO2 electrolyte of solid oxide fuel cells. Journal of Power Sources, 2018, 378, 433-442.	4.0	48
36	Precambrian reidite discovered in shocked zircon from the Stac Fada impactite, Scotland. Geology, 2015, 43, 899-902.	2.0	47

#	Article	IF	CITATIONS
37	Corrosion behaviour of nanocomposite TiSiN coatings on steel substrates. Corrosion Science, 2011, 53, 3678-3687.	3.0	46
38	Time-resolved, defect-hosted, trace element mobility in deformed Witwatersrand pyrite. Geoscience Frontiers, 2019, 10, 55-63.	4.3	44
39	Highly Stable Srâ€Free Cobaltiteâ€Based Perovskite Cathodes Directly Assembled on a Barrierâ€Layerâ€Free Y <sub>2</sub> O <sub>3</sub> â€ZrO <sub>2</sub> Electrolyte of Solid Oxide Fuel Cells. ChemSusChem, 2017, 10, 993-1003.	3.6	43
40	A FIB-STEM Study of Strontium Segregation and Interface Formation of Directly Assembled La <sub>0.6</sub> Sr <sub>0.4</sub> Co <sub>0.2</sub> Fe <sub>0.8</sub> O <sub>3-Î</sub> Cathode on Y <sub>2</sub> O <sub>3</sub> -ZrO <sub>2</sub> Electrolyte of Solid Oxide Fuel Cells. Journal of the Electrochemical Society, 2018, 165, F417-F429.	1.3	41
41	Assessment of a spodumene ore by advanced analytical and mass spectrometry techniques to determine its amenability to processing for the extraction of lithium. Minerals Engineering, 2018, 119, 137-148.	1.8	41
42	Characterization of various fly ashes for preparation of geopolymers with advanced applications. Advanced Powder Technology, 2013, 24, 495-498.	2.0	40
43	Nanoscale distribution of Pb in monazite revealed by atom probe microscopy. Chemical Geology, 2018, 479, 251-258.	1.4	39
44	Enhancing chalcopyrite leaching by tetrachloroethylene-assisted removal of sulphur passivation and the mechanism of jarosite formation. Hydrometallurgy, 2020, 191, 105192.	1.8	39
45	Aseismic Refinement of Orogenic Gold Systems. Economic Geology, 2020, 115, 33-50.	1.8	38
46	Three-dimensional quantification of pore structure in coal ash-based geopolymer using conventional electron tomography. Construction and Building Materials, 2014, 52, 221-226.	3.2	32
47	Novel Applications of FIB-SEM-Based ToF-SIMS in Atom Probe Tomography Workflows. Microscopy and Microanalysis, 2020, 26, 750-757.	0.2	32
48	Palaeobiology of red and white blood cell-like structures, collagen and cholesterol in an ichthyosaur bone. Scientific Reports, 2017, 7, 13776.	1.6	31
49	A new kind of invisible gold in pyrite hosted in deformation-related dislocations. Geology, 2021, 49, 1225-1229.	2.0	30
50	Acoustic emission and microstructural changes in fly ash geopolymer concretes exposed to simulated fire. Materials and Structures/Materiaux Et Constructions, 2016, 49, 5243-5254.	1.3	29
51	Organic matter network in post-mature Marcellus Shale: Effects on petrophysical properties. AAPG Bulletin, 2018, 102, 2305-2332.	0.7	28
52	Beneficiation of Collie fly ash for synthesis of geopolymer: Part 1 – Beneficiation. Fuel, 2013, 106, 569-575.	3.4	25
53	Thermal properties of geopolymers. , 2009, , 315-342.		24
54	In Situ Elevated Temperature Testing of Fly Ash Based Geopolymer Composites. Materials, 2016, 9, 445.	1.3	23

#	Article	IF	CITATIONS
55	Solar wind contributions to Earthâ $\in$ <sup>IM</sup> s oceans. Nature Astronomy, 2021, 5, 1275-1285.	4.2	22
56	Visualization of Diffusion within Nanoarrays. Analytical Chemistry, 2016, 88, 6689-6695.	3.2	20
57	The effects of particle angularity on low-stress three-body abrasion-corrosion of 316L stainless steel. Corrosion Science, 2016, 111, 690-702.	3.0	20
58	Volcanic SiO2-cristobalite: A natural product of chemical vapor deposition. American Mineralogist, 2020, 105, 510-524.	0.9	20
59	Applications of advanced analytical and mass spectrometry techniques to the characterisation of micaceous lithium-bearing ores. Minerals Engineering, 2018, 116, 182-195.	1.8	19
60	Direct Observation of Nanoparticulate Goethite Recrystallization by Atom Probe Analysis of Isotopic Tracers. Environmental Science & Technology, 2019, 53, 13126-13135.	4.6	19
61	Nanoscale constraints on the shock-induced transformation of zircon to reidite. Chemical Geology, 2019, 507, 85-95.	1.4	19
62	High performance anode with dendritic porous structure for low temperature solid oxide fuel cells. International Journal of Hydrogen Energy, 2018, 43, 17849-17856.	3.8	18
63	Effect of Volatile Boron Species on the Electrocatalytic Activity of Cathodes of Solid Oxide Fuel Cells. Journal of the Electrochemical Society, 2014, 161, F1163-F1170.	1.3	17
64	Optimising Ambient Setting Bayer Derived Fly Ash Geopolymers. Materials, 2016, 9, 392.	1.3	17
65	Positive Effect of Incorporating Er <sub>0.4</sub> Bi <sub>1.6</sub> O <sub>3</sub> on the Performance and Stability of La <sub>2</sub> NiO <sub>4+δ</sub> Cathode. Journal of the Electrochemical Society, 2019, 166, F796-F804.	1.3	17
66	Effect of Pd doping on the activity and stability of directly assembled La0.95Co0.19Fe0.76Pd0.05O3-δ cathodes of solid oxide fuel cells. Solid State Ionics, 2018, 316, 38-46.	1.3	16
67	Analysis of Natural Rutile (TiO <sub>2</sub> ) by Laser-assisted Atom Probe Tomography. Microscopy and Microanalysis, 2019, 25, 539-546.	0.2	16
68	Generation of amorphous carbon and crystallographic texture during low-temperature subseismic slip in calcite fault gouge. Geology, 2018, 46, 163-166.	2.0	15
69	Active, durable bismuth oxide-manganite composite oxygen electrodes: Interface formation induced by cathodic polarization. Journal of Power Sources, 2018, 397, 16-24.	4.0	15
70	Nanoscale Isotopic Dating of Monazite. Geostandards and Geoanalytical Research, 2020, 44, 637-652.	1.7	15
71	Facile co-synthesis and utilization of ultrafine and highly active PrBa0.8Ca0.2Co2O5+δ-Gd0.2Ce0.8O1.9 composite cathodes for solid oxide fuel cells. Electrochimica Acta, 2022, 403, 139673.	2.6	15
72	The effect of pre-treatment on the thermal performance of fly ash geopolymers. Thermochimica Acta, 2013, 573, 130-137.	1.2	14

#	Article	IF	CITATIONS
73	Understanding the Chemical and Structural Properties of Multiple-Cation Mixed Halide Perovskite. Journal of Physical Chemistry C, 2019, 123, 26718-26726.	1.5	14
74	Effects of waste glass sand on the thermal behavior and strength of fly ash and GGBS based alkali activated mortar exposed to elevated temperature. Construction and Building Materials, 2022, 316, 125864.	3.2	14
75	The Influence of Short Fibres and Foaming Agents on the Physical and Thermal Behaviour of Geopolymer Composites. Advances in Science and Technology, 0, , .	0.2	13
76	Nebula sulfidation and evidence for migration of "free-floating―refractory metal nuggets revealed by atom probe microscopy. Geology, 2017, 45, 847-850.	2.0	13
77	Defining the Potential of Nanoscale Reâ€Os Isotope Systematics Using Atom Probe Microscopy. Geostandards and Geoanalytical Research, 2018, 42, 279-299.	1.7	13
78	A new method for dating impact events – Thermal dependency on nanoscale Pb mobility in monazite shock twins. Geochimica Et Cosmochimica Acta, 2021, 314, 381-396.	1.6	13
79	Mineralogy of Al-substituted goethites. Powder Diffraction, 2006, 21, 289-299.	0.4	12
80	Dislocations in minerals: Fast-diffusion pathways or trace-element traps?. Earth and Planetary Science Letters, 2022, 584, 117517.	1.8	12
81	Other Potential Applications for Alkali-Activated Materials. RILEM State-of-the-Art Reports, 2014, , 339-379.	0.3	11
82	Hall–Petch Slope in Ultrafine Grained Al-Mg Alloys. Metallurgical and Materials Transactions A: Physical Metallurgy and Materials Science, 2019, 50, 4047-4057.	1.1	11
83	Standardizing Spatial Reconstruction Parameters for the Atom Probe Analysis of Common Minerals. Microscopy and Microanalysis, 2022, 28, 1221-1230.	0.2	11
84	A Review on Geopolymer Technology for Lunar Base Construction. Materials, 2022, 15, 4516.	1.3	11
85	Life on the edge: Microbial biomineralization in an arsenic- and lead-rich deep-sea hydrothermal vent. Chemical Geology, 2020, 533, 119438.	1.4	10
86	Disorientation control on trace element segregation in fluid-affected low-angle boundaries in olivine. Contributions To Mineralogy and Petrology, 2021, 176, 1.	1.2	10
87	Xenotime at the Nanoscale: Uâ€₱b Geochronology and Optimisation of Analyses by Atom Probe Tomography. Geostandards and Geoanalytical Research, 2021, 45, 443-456.	1.7	10
88	Assessment of Residual Strain in Zirconia-Toughened Alumina Using Neutron Diffraction. Journal of the American Ceramic Society, 1993, 76, 2133-2135.	1.9	9
89	Characterization of Ceramic Materials with BIGDIFF: A Synchrotron Radiation Debye cherrer Powder Diffractometer. Journal of the American Ceramic Society, 1997, 80, 1373-1381.	1.9	9
90	Lunar samples record an impact 4.2 billion years ago that may have formed the Serenitatis Basin. Communications Earth & Environment, 2021, 2, .	2.6	9

#	Article	IF	CITATIONS
91	Pre-nucleation geochemical heterogeneity within glassy anatectic inclusions and the role of water in glass preservation. Contributions To Mineralogy and Petrology, 2021, 176, 1.	1.2	8
92	Corrosion―and Damageâ€Resistant Nitride Coatings for Steel. Journal of the American Ceramic Society, 2012, 95, 2997-3004.	1.9	7
93	Atom probe microscopy of zinc isotopic enrichment in ZnO nanorods. AIP Advances, 2017, 7, .	0.6	7
94	Crystallography of refractory metal nuggets in carbonaceous chondrites: A transmission Kikuchi diffraction approach. Geochimica Et Cosmochimica Acta, 2017, 216, 42-60.	1.6	7
95	Developing Atom Probe Tomography of Phyllosilicates in Preparation for Extraâ€Terrestrial Sample Return. Geostandards and Geoanalytical Research, 2021, 45, 427-441.	1.7	5
96	Variability of sulfur isotopes and trace metals in pyrites from the upper oceanic crust of the South China Sea basin, implications for sulfur and trace metal cycling in subsurface. Chemical Geology, 2022, 606, 120982.	1.4	5
97	Microstructural and Chemical Investigations of Presolar Silicates from Diverse Stellar Environments. Astrophysical Journal, 2022, 925, 110.	1.6	4
98	Ion-transfer electrochemistry at arrays of nanoscale interfaces between two immiscible electrolyte solutions arranged in hexagonal format. Journal of Electroanalytical Chemistry, 2022, 909, 116113.	1.9	3
99	Correlative Analysis using FIB-ToF-SIMS and Atom Probe Tomography on Geological Materials. Microscopy and Microanalysis, 2016, 22, 684-685.	0.2	2
100	Low Stress Abrasion-Corrosion of High-Cr White Cast Iron: Combined Effects of Particle Angularity and Chloride Ions. Journal of the Electrochemical Society, 2019, 166, C382-C393.	1.3	1
101	Substructural phenomena in Cu wire bond after laser assisted manufacturing in electronic packaging. Materials Letters, 2020, 259, 126833.	1.3	1
102	Rapid prototyping of grating magneto-optical traps using a focused ion beam. Optics Express, 2021, 29, 37733.	1.7	1
103	Three-body abrasion-corrosion behaviour of as printed and solution annealed additively manufactured 316L stainless steel. Corrosion, 0, , .	0.5	Ο